Title

Optimizing trajectory ordering for fast radial ultra-short TE (UTE) acquisitions

Permalink

https://escholarship.org/uc/item/1qd2c93p

Authors

Zhu, Xucheng
Tan, Fei
Johnson, Kevin
et al.

Peer reviewed

Optimizing trajectory ordering for fast radial ultra-short TE (UTE) acquisitions

Xucheng Zhu[a,b,c], **Fei Tan**[a,b], **Kevin Johnson**[d,e], **Peder Larson**[a,b,*]

[a]UC Berkeley-UCSF Graduate Program in Bioengineering, University of California, San Francisco and University of California, Berkeley, CA, United States

[b]Radiology and Biomedical Imaging, University of California, San Francisco, CA, United States

[c]GE Healthcare, Menlo Park, CA, United States

[d]Medical Physics, University of Wisconsin, Madison, WI, United States

[e]Radiology, University of Wisconsin, Madison, WI, United States

Abstract

Purpose: Additional spoiler gradients are required in 3D UTE sequences with random view ordering to suppress magnetization refocusing. By leveraging the encoding gradient induced spoiling effect, the spoiler gradients could potentially be reduced or removed to shorten the TR and increase encoding efficiency. An analysis framework is built that models the gradient spoiling effects and a new ordering scheme is proposed for fast 3D UTE acquisition.

Theory and methods: UTE signal evolution and spatial encoding gradient induced spoiling effect are derived from the Bloch equations. And the concept is validated in 2D radial UTE simulation. Then an optimized ordering scheme, named reordered 2D golden angle (r2DGA) scheme, for 3D UTE acquisition is proposed. The r2DGA scheme is compared to the sequential and 3D golden angle schemes in both phantom and volunteer studies.

Results: The proposed r2DGA ordering scheme was applied to two applications, single breath-holding and free breathing 3D lung MRI. With r2DGA ordering scheme, breath-holding lung MRI scan increased 60% scan efficiency by removing the spoiler gradients and the free breathing scan reduced 20% scan time compared to the 3D golden angle scheme by reducing the spoiler gradients.

Conclusions: The proposed r2DGA ordering scheme UTE acquisition reduces the need of spoiler gradients and increases the encoding efficiency, and shows improvements in both breath-holding and free breathing lung MRI applications.

Keywords

Non-Cartesian MRI; UTE; Lung MRI

1. Introduction

Ultra-short echo time (UTE) MRI exhibits great promise in imaging short T2* components in tissues, such as bone [1], lung [2–3], etc. To achieve the shortest TE, UTE sequences usually start acquisition right after the RF excitation from the center of k-space. Center-out radial acquisition is a widely used trajectory for UTE acquisition. There are several benefits of using a radial type trajectory, such as a simple gradient design, robustness to chemical shift and B0 inhomogeneity, etc.

One major application of UTE sequences is lung MRI. However, 3D UTE acquisitions usually take a few minutes to achieve high resolution imaging, which is usually challenging to acquire under breath-holding conditions. To increase the robustness to respiratory motion, random or pseudo-random ordering schemes have been applied to UTE design [4–6]. One of the widely used pseudo-random ordering schemes is golden angle ordering scheme [7]. The original golden angle scheme was designed for 2D radial or 3D stack-of-stars trajectories [8]. Recently, a 3D golden angle scheme using two golden ratios was proposed for the 3D koosh ball radial trajectory [9].

Like standard GRE sequences, UTE sequences usually require a large spoiler gradient before each TR to dephase the residual transverse magnetization from previous TRs. However, spoiler gradients prolong the TR and reduce the encoding efficiency [10–11]. RF spoiling strategy is another widely used spoiling strategy, which changes the phase of RF excitation pulse TR by TR [12–13] to cancel the effects of residual transverse magnetizations, however, it still requires an extra rewinding gradient to refocus the magnetization. Gradient and RF spoiling strategies are often used together to suppressed the residual signals [14–16]. Lin proposed to combine randomized RF phases with strong spoiler gradient to achieve a pseudo steady state with very slight fluctuation [14]. However, even with RF spoiling strategies, spoiler and rewinder gradients are still needed in UTE sequences.

To reduce the total acquisition time and increase scan efficiency, strategies that can reduce or even remove spoiler gradients should be considered. Similar ideas have been used in zero TE (ZTE) sequences [17–18]. In ZTE, encoding gradients are adjusted slightly between the successive excitations, and a short waiting time is added to the end of acquisition to serve as a small spoiler gradient. This scheme could be also applied to UTE acquisitions to reduce or remove spoiler gradients. In addition, adding RF spoiling strategies to the sequence might further improve the spoiling effects. Roeloffs et al., investigated the effect of view ordering on spoiler gradient free 2D radial MRI with randomized RF phases [19]. Compared to the ordering schemes with large trajectory angle changes, such as the golden angle scheme, small incremental angle radial schemes show much lower artifact levels in the final images. In addition, scan efficiency of UTE acquisition could be also improved from other aspects. Idiyatullin proposed a fast and silent imaging method called SWIFT to image short

T2components [20]. Willmering et al., used FLORET (Fermat looped, orthogonally encoded trajectories) for high efficiency lung MRI [21]. And Delacoste et al., proposed a dual echo UTE sequence to improve scan efficiency for lung MRI [22].

In this work, we firstly demonstrate how different ordering schemes affect the gradient spoiling effects of the center-out radial UTE acquisition. Then, we propose a new ordering scheme, called reordered 2D golden angle (r2DGA), to smoothly adjust encoding gradient moments while maintaining the robustness to respiratory motion for 3D UTE acquisitions. The proposed r2DGA is compared to the sequential and 3D Golden Angle (3DGA) ordering schemes. We evaluated the proposed method in volunteer lung imaging studies. The results show improvements by using the proposed r2DGA scheme in breath-holding acquisition because of approximately 60% higher encoding efficiency and comparable image quality in the free breathing acquisition with up to a 20% scan time reduction.

2. Theory

2.1. Signal evolution in spoiler gradient free UTE

To describe the refocusing and dephasing phenomena of the transverse magnetization in UTE sequence, the sequence can be decomposed into three components: RF excitation, gradient effects, and "other" (including relaxation, diffusion, and exchange etc.). According to the Bloch equations [23–24], the RF excitation effect on the magnetization is given by:

$$\begin{bmatrix} M_+ \\ M_- \\ M_z \end{bmatrix}_{n+1} = \begin{bmatrix} \cos^2\frac{\alpha}{2} & e^{2i\Phi}\sin^2\frac{\alpha}{2} & -ie^{i\Phi}\sin\alpha \\ e^{-2i\Phi}\sin^2\frac{\alpha}{2} & \cos^2\frac{\alpha}{2} & ie^{-i\Phi}\sin\alpha \\ -\frac{i}{2}e^{-i\Phi}\sin\alpha & \frac{i}{2}e^{i\Phi}\sin\alpha & \cos\alpha \end{bmatrix}\begin{bmatrix} M_+ \\ M_- \\ M_z \end{bmatrix}_n = R_{n+1}\begin{bmatrix} M_+ \\ M_- \\ M_z \end{bmatrix}_n \tag{1}$$

Here $[M_+, M_-, M_z]_n^T$ and $[M_+, M_-, M_z]_{n+1}^T$ are the magnetization before and after the (n + 1)th RF pulse, α and Φ are flip angle and phase of the RF pulse. M_z is the longitudinal magnetization. M_+ and M_-, represent the transverse magnetization, which can be converted to M_x, and M_y via a unitary transformation [25].

Gradient effects can be formulated as a diagonal matrix multiplication, which apply a phase accumulation on the transverse magnetizations.

$$\begin{bmatrix} M_+ \\ M_- \\ M_z \end{bmatrix}_n = \begin{bmatrix} e^{i\gamma\int_{TR_{n-1}}^{TR_n}G(t)rdt} & 0 & 0 \\ 0 & e^{-i\gamma\int_{TR_{n-1}}^{TR_n}G(t)rdt} & 0 \\ 0 & 0 & 1 \end{bmatrix}\begin{bmatrix} M_+ \\ M_- \\ M_z \end{bmatrix}_n$$
$$= P_n\begin{bmatrix} M_+ \\ M_- \\ M_z \end{bmatrix}_n \tag{2}$$

Here, the $G(t)$ and r represent spatial encoding gradient and spatial location vectors. And we use the k-space notation $k_n = \int_{TR_{n-1}}^{TR_n} \frac{\gamma}{2\pi} G(t) dt$ in the following analysis.

Similarly, relaxations could be formulated as below,

$$
\begin{bmatrix} M_+ \\ M_- \\ M_z \end{bmatrix}_n = \begin{bmatrix} e^{-\frac{TR}{T2}} & 0 & 0 \\ 0 & e^{-\frac{TR}{T2}} & 0 \\ 0 & 0 & -e^{\frac{TR}{T1}} \end{bmatrix} \begin{bmatrix} M_+ \\ M_- \\ M_z \end{bmatrix}_n + \begin{bmatrix} 0 \\ 0 \\ M_0\left(1 - e^{-\frac{TR}{T1}}\right) \end{bmatrix} = A \begin{bmatrix} M_+ \\ M_- \\ M_z \end{bmatrix}_n + B \tag{3}
$$

Here, T_1 and T_2 are the relaxation times, and TR is the repetition time. As for diffusion, we assume a Gaussian diffusion model, where K is the accumulated k-space location and is equal to $K(t, t_0) = \int_{t_0}^{t} \frac{\gamma}{2\pi} G(\tau) \tau$. Here, t_0 is the time right after excitation and t represents the current acquisition time. And the overall diffusion effect can be also written as a diagonal matrix with decay on transverse components.

$$
\begin{bmatrix} M_+ \\ M_- \\ M_z \end{bmatrix}_n =
$$

$$
\begin{bmatrix} e^{-4\pi^2 D \int_{TR_{n-1}}^{TR_n} |K(t, t_0)|^2 dt} & 0 & 0 \\ 0 & e^{-4\pi^2 D \int_{TR_{n-1}}^{TR_n} |K(t, t_0)|^2 dt} & 0 \\ 0 & 0 & 1 \end{bmatrix} \tag{4}
$$

$$
\begin{bmatrix} M_+ \\ M_- \\ M_z \end{bmatrix}_n = D_n \begin{bmatrix} M_+ \\ M_- \\ M_z \end{bmatrix}_n
$$

Now, we can now ensemble the aforementioned components, Equation (1–4), together.

$$
M_{n+1} = D_{n+1} P_{n+1} (A R_{n+1} M_n + B) \tag{5}
$$

Here, we use M to represent magnetization vector $[M_+, M_-, M_z]^T$.

In this work, we simplify the formulation based on a few assumptions for the following gradient spoiling analysis.

According to Equation (1), RF pulse results in splitting the isochromat magnetization M_+ to three components [25], rephasing, and dephasing transverse magnetization and longitudinal magnetization. The proportions of different components depend on the flip angle α. And the relationship between flip angle and the split signals is plotted in Supporting Information Fig. 1. In the context of the UTE sequence, the flip angle is usually set to be very small, usually smaller than 6° [26]. Under that assumption, the refocusing signal is only 0.27% of the total transverse magnetization before the RF excitation, thus it will be ignored in the following analysis.

In addition, chemical exchange effects are also ignored under the small flip angle condition, resulting in the following simplification of Equation (1):

$$
\begin{bmatrix}
\cos^2\frac{\alpha}{2} & e^{2i\Phi}\sin^2\frac{\alpha}{2} & -ie^{i\Phi}\sin\alpha \\
e^{-2i\Phi}\sin^2\frac{\alpha}{2} & \cos^2\frac{\alpha}{2} & ie^{-i\Phi}\sin\alpha \\
-\frac{i}{2}e^{-i\Phi}\sin\alpha & \frac{i}{2}e^{i\Phi}\sin\alpha & \cos\alpha
\end{bmatrix}
\approx
\begin{bmatrix}
1 & 0 & -ie^{i\Phi}\alpha \\
0 & 1 & ie^{-i\Phi}\alpha \\
-\frac{i}{2}e^{-i\Phi}\alpha & \frac{i}{2}e^{i\Phi}\alpha & 1
\end{bmatrix}
\tag{6}
$$

Combining Equations (2), (3), (5), and (6), we get:

$$
\begin{aligned}
M_{n+1} &\approx
\begin{bmatrix}
e^{i2\pi k_n \cdot r}e^{-\frac{t}{T_2}} & 0 \\
0 & e^{-i2\pi k_n \cdot r}e^{-\frac{t}{T_2}}
\end{bmatrix}
\begin{bmatrix}
-ie^{i\Phi}\alpha M_z \\
ie^{-i\Phi}\alpha M_z
\end{bmatrix}_n \\
&+
\begin{bmatrix}
e^{i2\pi k_n \cdot r}e^{-\frac{t}{T_2}} & 0 \\
0 & e^{-i2\pi k_n \cdot r}e^{-\frac{t}{T_2}}
\end{bmatrix}
e^{-4\pi^2 D\int_{TR_n}^{TR_n+1}|K(t,TR_n)|^2 dt} M_n
\end{aligned}
\tag{7}
$$

Here, we use M to represent transverse magnetization $[M_+, M_-]^T$. M_{n+1} can be separated to two terms, the new excitation magnetization (the first row, desired signal), and the previous transverse magnetization (the second row, undesired residual signal).

When the residual transverse magnetizations from all the previous TRs are included, the undesired residual signal could be written as below:

$$
\begin{aligned}
dM_n &= \sum_{i=1}^{n}
\begin{bmatrix}
e^{i2\pi\sum_{t-i}^{n} k_t \cdot r}e^{-\frac{t}{T_2}} & 0 \\
0 & e^{-i2\pi\sum_{t-i}^{n} k_t \cdot r}e^{-\frac{t}{T_2}}
\end{bmatrix} \\
&\quad e^{-4\pi^2 D\int_{TR_i}^{TR_n+1}|K(t,TR_n)|^2 dt}
\begin{bmatrix}
-ie^{i\Phi}\alpha M_z \\
ie^{-i\Phi}\alpha M_z
\end{bmatrix}_i
\end{aligned}
\tag{8}
$$

The total residual signal, dM_n, is the sum of all the residual signals from certain TR is indexed by i. And each component has an accumulated phase and an extra diffusion term.

The accumulated phases as well as diffusion effects on the previous transverse magnetizations depends on K_n^i, given by:

$$K_n^i = K(TR_n, TR_i) = \sum_{t=i}^{n} k_t \qquad (9)$$

According to Equation (8) and (9), the same sampling pattern design would create different K series by changing the sampling order. A large $\left|K_n^i\right| (for i \in [1, 2, \cdots, n])$ series would induce a strong dephasing effect as well as a large diffusion effect to suppress the previous residual transversion magnetizations. Therefore, the ordering scheme design plays an important role in spoiler gradient free UTE.

In this study, dephasing effects are mainly contributed from the encoding gradient spoiling, therefore, the associated diffusion effect of the encoding gradients is not further discussed in this work.

The magnitude of spoiling moment induced by an individual encoding gradient is constant for center-out radial sequences, which equals to the maximum extent in k-space. To simplify the analysis, we note the spoiling moment induced by a single encoding gradient as one π, representing a π dephasing effect across one voxel.

2.2. Simulation

A 2D center-out radial sequence with 20 radial spokes was simulated to show how different radial ordering schemes affect the spoiler gradient free UTE sequence. Two ordering schemes, sequential and golden angle ordering, are compared in Fig. 1. Trajectory orderings are color-encoded, plotted in (a), and the respective pulse sequence sketches are plotted in (b). The accumulated gradient spoiling moments evolutions of each excitation, calculated from Equations (6)–(8), are plotted in (c). The sequential ordering scheme has a smooth change of the readout gradient moment, which increases the accumulated spoiling moments to dephase the residual transverse signals. In contrast, the golden angle scheme partially refocuses residual transverse signals from previous TRs leading to signal contamination. In addition, larger accumulated gradient spoiling moments of the sequential ordering scheme are associated with stronger diffusion effects, which would further attenuate the residual transverse signals.

A simple digital simulation with a 2D uniform circle phantom is shown in Fig. 1 (d). The observed signals from one readout of simulation are plotted in (e), and the signals are decomposed to signals from different excitations according to (b). With the sequential scheme, the residual signals are suppressed, the observed signal is well-aligned with the desired signal. However, with the golden angle scheme, the observed signal is largely corrupted by refocused residual signals. The final reconstruction images from the simulation are compared in (f). The reference image is reconstructed with simulated data without the residual signal corruption. The image with sequential ordering more effectively suppresses the artifacts induced by residual signal compared to golden angle scheme.

We also investigated the effect of T2 decay and using RF spoiling, plotted in Supporting Information Fig. 2. As T2 increases, refocusing magnetization induced artifacts are stronger with the golden angle ordering scheme. With sequential ordering scheme, only very slight artifacts are shown even with long T2s. And adding extra RF spoiling also helps further reduce the artifacts, especially for longer T2 situations. Therefore, quadratic phase RF spoiling strategy is added to the later phantom and volunteer studies as default.

Similar to 2D, 3D radial ordering design could be also analyzed under the same framework, and encoding gradients should be changed smoothly to dephase the residual transverse signals.

2.3. View ordering design for 3D UTE acquisition

As mentioned before, to maximize the gradient spoiling moments of the spoiler free 3D UTE sequence, the encoding gradients should be smoothly changed. Sequential ordering, similar to the 2D example above, is one of the candidates fulfilling the requirement. However, fully sequential ordering is not as robust to subject motion when compared to golden angle ordering. With golden angle ordering, data can also be arbitrarily reorganized for retrospective motion correction while maintaining a uniform sampling distribution. As for 3D acquisitions, to balance the robustness to motion and smoothness of the readout direction changes, we propose r2DGA scheme to combine a through-plane (z-axis) continuous acquisition with an in-plane golden angle acquisition scheme. The pseudo code for ordering design is shown below.

```
Initialization:
3D radial design scheme:
[xi, yi, zi], xi² + yi² + zi² = 1,   i ∈ 1, 2, ···, N
η = 0.618, Ng number of groups,
    Gi  (i ∈ 1, 2, ···, N) group index.
for i = 1 : N
    θi = arctan(x[i]/y[i])
    G[i] =      argmax       cos(θi, θk)
              θk = 2πηk,
           k ∈ (1, 2, ···Ng)
end
for k = 1 : Ng
    if  k is odd, [x, y, z]i with G[i] = k are sorted by z
    in descending order
    if  k is even, [x, y, z]i with G[i] = k are sorted by z
       in ascending order
end
```

For comparison, two other view ordering schemes, the sequential ordering, and the 3D golden angle (3DGA) schemes [5], are used in this work, ordering design schemes are summarized in Supporting Information Table 1.

To quantify the sampling uniformity over time of different acquisition schemes, we define a metric named maximum minimum distance (MMD) of sampling pattern.

$$MMD = \max_{j \in J} \min_{i \in I_{sub}} dist[e(\theta_i, \phi_i), e(\theta_j, \phi_j)] \tag{10}$$

Here, θ and ϕ are two design variables in radial ordering design. And the first term $e(\theta_i, \phi_i)$ represents sample of a subset $\boldsymbol{I}_{sub}$ of designed sampling schemes within certain time window, for instance, 1000 continuous spokes out of a 100,000 spokes acquisition. The second term $e(\theta_j, \phi_j)$ is a sample from the predefined uniform sampling pattern $\boldsymbol{J}$ on the sphere. And $dist[\cdot, \cdot]$ is orthodromic distance between two samples on the unit sphere. Smaller MMD indicates more uniform temporal sampling.

1000 continuously acquired spokes out of the total 100,000 spokes with three ordering schemes are plotted in Fig. 2 (a). The average accumulated spoiling moments of transverse magnetization in the following TRs are used to evaluate the accumulated spoiling effects, as plotted in (c). Similar to the 2D simulation results, the 3DGA scheme generates small accumulated spoiling moments which might not be enough to dephase residual transverse magnetizations without spoiler gradients. In contrast, the sequential and r2DGA schemes generate much larger spoiling moments to dephase the residual signals. In addition, the comparison of MMD on 1000 continuously acquired spokes over time with different ordering schemes plotted in (d) indicates r2DGA and 3DGA have much more uniform temporal sampling patterns than the sequential scheme.

One tunable parameter in r2DGA design algorithm is the number of spokes per group. 1000 continuous spokes with 6 different number of spokes per group are plotted in Fig. 3 (a), and the average accumulated spoiling moments are plotted in (b) accordingly. As the number of spokes per group increases, the average accumulated spoiling moments also increase in the subsequent TRs. Mean-while, sampling pattern with more spokes per group are less uniformly distributed with smaller MMDs, according to (c).

3. Methods

3.1. MRI experiments

All experiments were run on a 3 T MR scanner (General Electric, Milwaukee, WI) with a 32-channel phased array cardiac coils. An optimized variable density readout center-out radial UTE sequence [4] was used in all the experiments. The 3DGA ordering sequence with the same field of view (FOV), spatial resolution, and sampling bandwidth as other scans with 4π spoiler gradient was acquired as the reference for both phantom and in vivo studies. And the quadratic phase RF spoiling strategy was applied to all the scans.

3.2. Phantom study

A multi-purpose phantom was used in the phantom experiments. Data were acquired with 1 mm isotropic resolution, image matrix size $200 \times 200 \times 200$, TE = 100 μs, readout bandwidth = 125 kHz, TR = 2.2 ms. UTE sequences with sequential, 3DGA and the proposed r2DGA ordering schemes acquired without a spoiler gradient were compared. All three sequences were acquired with 100,000 spokes.

Different scale spoiler gradients, 1 π and 4 π are combined with different ordering schemes and different numbers of spokes per group are used for r2DGA ordering in a phantom study.

3.3. Human study

All the volunteer studies conducted were approved by UCSF Institutional Review Board (IRB). Two types of acquisitions were designed for human studies: a free breathing scan and a breath-holding scan.

For free breathing scans, data were acquired with 1.25 mm isotropic spatial resolution, image matrix size $256 \times 256 \times 256$, TE = 70 μs, 100,000 spokes, with approximately 2-fold undersampling. Motion corrected images were reconstructed with the self-navigated soft-gating reconstruction [27]. The TRs depended on the moments of the spoiler gradient, ranging between 1.9 and 3.7 ms, and the flip angles were set to 4–6° accordingly to target Ernst angle with 1 s T1.

For breath-holding scans, data were acquired with 2 mm isotropic spatial resolution, image matrix size reduced to $160 \times 160 \times 160$, TE = 70 μs, the TRs ranged between 1.5 and 2.5 ms. And number of spokes were calculated to fit the whole sequence in 15 s. 3DGA scheme with 4π spoiler gradient acquired ~6000 spokes, and r2DGA schemes without spoiler gradient acquired ~10,000 spokes in 15 s. Assuming little respiratory motion in the breath-holding scans, direct NUFFT with density compensation followed by coil combination reconstruction was used without any motion correction.

For both applications, the number of spokes per group in r2DGA design was set to 50 targeting at around 100 ms acquisition time per group, which is much faster than the respiration rate, and the number of groups is total spokes divided by number of spokes per group.

4. Results

4.1. Phantom study

Single axial slices at the same location from a phantom using 3DGA with 4π spoiler gradient, 3DGA and r2DGA without spoiler gradient, are shown in Fig. 4. Compared to 3DGA without spoiler gradient, the r2DGA ordering scheme largely suppresses the unwanted residual transverse signals and has a much lower root mean square error (RMSE).

In Supporting Information Fig. 6, image acquired with r2DGA ordering with 1π spoiler gradient shows less artifacts than 3DGA ordering with the same spoiler gradient scale, which indicates 3DGA needs larger spoiler gradient to suppress residual signals.

Another phantom experiment is designed to evaluate how number of spokes per group affects spoiling effect, and results are summarized in Supporting Information Fig. 4. By using 250, 100, and 50 spokes per group for the phantom study, images are with comparable image quality compared to reference scan, and the signal standard deviations are slightly higher than the reference. As the number of spokes per group further decreases to 25, image artifacts are more obvious, and the signal standard deviation largely increases. However, there is a trade-off between motion robustness and sampling continuity. We also evaluate the motion robustness of r2DGA ordering with 50 spokes per group, which is used in *in vivo* studies, in a simulated free breathing acquisition on phantom. Fully sampled datasets are

retrospectively gated based on different simulated respiratory rates, and the gated data are used to reconstruct simulated motion free images for motion robustness comparison, and details are summarized in Supporting Information Fig. 5. Both images with r2DGA and 3DGA ordering schemes show motion robustness to different respiratory rates. However, strong aliasing artifacts are observed on images with sequential ordering scheme.

4.2. Breath-holding study

Eliminating the spoiler gradient is valuable to shorten the TR and increase total number of spokes acquired for breath-holding scans. Fig. 5 shows a 15-s breath-holding acquisition with two different acquisition schemes at inspiration and expiration. With 4π spoiler gradient, the 3DGA sequence could acquire ~6000 spokes in 15 s, and has approximately 12-fold undersampling. In contrast, the r2DGA acquisition without spoiler gradient can fit ~10,000 spokes within the same duration, reducing the undersampling factor to around 7.2. Much less streaking artifacts are observed with the r2DGA spoiler free acquisition compared to with the standard 3DGA scheme. Small anatomical structures, such as vessels and airways, as well as the lung parenchyma that has low proton density (pointed out by red arrows) are also better delineated with the r2DGA spoiler free acquisition.

4.3. Free-breathing study

As shown in Fig. 4, there are still slight artifacts shown on the image without spoiler gradient. Therefore, spoiler gradients with varied scales were added to suppress the residual signals. Images acquired in a healthy volunteer with the 3DGA ordering with 4π spoiler gradient (reference), the r2DGA without a spoiler gradient, and the r2DGA with 1π spoiler gradient are shown in Fig. 6. The r2DGA acquisition without the spoiler gradient reduced the scan time by 40% compared to the reference scan. However, slight noise-like artifacts show up in the images with the spoiler free acquisition, which make small airways difficult to distinguish from the lung parenchyma (pointed out by orange arrows). By adding a 1π spoiler gradient to the r2DGA sequence, these artifacts are largely suppressed, and image quality, such as aorta aSNR is comparable to reference scan but with a 20% reduction in scan time compared to the 3DGA reference scan. Maximum intensity projection (MIP) maps of 15 coronal slices from each acquisition are shown in (b), further demonstrating that the r2DGA with 1π spoiler gradient largely reduce the artifacts seen without a spoiler gradient and preserves more fine structures, pointed out by red arrows.

5. Discussion

In this work, we demonstrated how 3D center-out radial UTE ordering affects the transverse magnetization spoiling and proposed a new reordering scheme named reordered 2D Golden Angle scheme for 3D UTE to reduce the need for a spoiler gradient. Compared to the 3D golden angle scheme, the proposed r2DGA changes the encoding gradient amplitudes much more smoothly, inducing larger spoiling moments and diffusion effects between TRs to help suppress the residual transverse magnetization. In addition, the r2DGA scheme still samples randomly in two dimensions to keep uniform sampling distributions and robustness to subject motion. The number of spokes per group is a tunable parameter in the r2DGA design

algorithm. By reducing the number of spokes per group, sampling pattern is more uniform in k-space, but the induced spoiling moments and diffusion effects decrease.

When comparing the images acquired with and without spoiler gradients, slight artifacts were observed in the images without spoiler gradient. This suggests that even with smoothly changing the trajectory directions, the residual transverse magnetizations from adjacent TRs are not fully spoiled which creates these artifacts. To suppress the residual magnetizations, we found that small spoiler gradients were still needed.

In this work, we limited analysis of the residual transverse magnetizations evolution to just the gradient spoiling moments, but they also largely depend on the subject structure as well as T1 and T2 relaxation rates. In fact, the accumulated spoiling moments of the transverse magnetization could be treated as sampling k-space at very high frequencies. We assumed the signal intensity decreases as the spoiling moment increases (high frequency components in the k-space), regardless of the diffusion effect. If the subject has repeated high frequency structure they could be sampled by the accumulated readout gradients and the residual transverse magnetizations might still corrupt the signals in the following TRs.

As we mentioned before, we ignored the refocusing component of the magnetization because of small tip excitation, which is typically used in 3D UTE sequences. As for larger flip angles, the assumption that refocusing magnetization is negligible no longer holds. Under that situation, smoothly changing the trajectory directions would refocus the refocusing magnetization instead of dephasing it according to Equation (1). To suppress both refocusing and dephasing residual magnetizations under larger flip angle situations, a comprehensive strategy including diffusion, gradient spoiling and RF spoiling strategies is needed [28].

In this work, the proposed ordering design is one of the options for free breathing acquisition. According to the gradient spoiling analysis, the ordering design could also be formulated as an optimization problem, with certain sampling criteria, such as uniformity of the sampling scheme, which could be generalized for broader applications. By solving the optimization problem, an optimal ordering scheme can be achieved. However, as the number of radial spokes increases, the computational complexity of the problem grows quickly.

Phyllotaxis spiral ordering [6] with interleaving, which was developed for cardiac bSSFP sequences to reduce eddy currents, also has the smooth gradient displacements property. It could be also adapted to UTE acquisition with slight modifications [29]. Because the proposed r2DGA method is a reordering method, compared to interleaved phyllotaxis spiral ordering, it can be more easily adapted to include other features, such as anisotropic FOV radial acquisition [30–31].

Besides the center-out radial trajectory demonstrated, cones [32], radial cones [33], and FLORET [34] trajectories have also been used successfully for 3D UTE acquisitions. Because of their curvature in k-space compared to the center-out radial trajectory, acquisitions without spoiler gradients might have additional refocusing of the transverse magnetization during the readout and these trajectories were out of scope.

6. Conclusion

In this work, we analyze how ordering schemes affect transverse magnetization spoiling in UTE acquisitions, and propose a new ordering scheme, named reordered 2D golden angle (r2DGA), for 3D UTE sequences to reduce the spoiler gradient requirements and increase the encoding efficiency. With r2DGA ordering scheme, we achieve a comparable image quality to the typical 3DGA ordering scheme in a free breathing lung scan but shortened the scan time by 20%. The proposed r2DGA scheme also improves a breath-holding lung scan because of its shorter TR and 60% higher encoding efficiency compared to the 3DGA ordering sequence that requires large spoiler gradients.

Supplementary Material

Refer to Web version on PubMed Central for supplementary material.

Funding

References

[1]. Du J, Carl M, Bydder M, Takahashi A, Chung CB, Bydder GM, Qualitative and quantitative ultrashort echo time (UTE) imaging of cortical bone, J. Magn. Reson 207 (2) (2010) 304–311, 10.1016/j.jmr.2010.09.013. [PubMed: 20980179]

[2]. Togao O, Tsuji R, Ohno Y, Dimitrov I, Takahashi M, Ultrashort echo time (UTE) MRI of the lung: assessment of tissue density in the lung parenchyma, Magn. Reson. Med 64 (5) (2010) 1491–1498, 10.1002/mrm.22521. [PubMed: 20574988]

[3]. Kveder M, Zupančič I, Lahajnar G, et al., Water proton NMR relaxation mechanisms in lung tissue, Magn. Reson. Med 7 (4) (1988) 432–441, 10.1002/mrm.1910070406. [PubMed: 3173058]

[4]. Johnson KM, Fain SB, Schiebler ML, Nagle S, Optimized 3D ultrashort echo time pulmonary MRI, Magn. Reson. Med 70 (5) (2013) 1241–1250, 10.1002/mrm.24570. [PubMed: 23213020]

[5]. Chan RW, Ramsay EA, Cunningham CH, Plewes DB, Temporal stability of adaptive 3D radial MRI using multidimensional golden means, Magn. Reson. Med 61 (2) (2009) 354–363, 10.1002/mrm.21837. [PubMed: 19165897]

[6]. Piccini D, Littmann A, Nielles-Vallespin S, Zenge MO, Spiral phyllotaxis: the natural way to construct a 3D radial trajectory in MRI, Magn. Reson. Med 66 (4) (2011) 1049–1056, 10.1002/mrm.22898. [PubMed: 21469185]

[7]. Winkelmann S, Schaeffter T, Koehler T, Eggers H, Doessel O, An optimal radial profile order based on the golden ratio for time-resolved MRI, IEEE Trans. Med. Imaging 26 (1) (2007) 68–76, 10.1109/TMI.2006.885337. [PubMed: 17243585]

[8]. Feng L, Axel L, Chandarana H, Block KT, Sodickson DK, Otazo R, XD-GRASP: Golden-angle radial MRI with reconstruction of extra motion-state dimensions using compressed sensing, Magn. Reson. Med (October 2014) (2015), 10.1002/mrm.25665.

[9]. Chan RW, Ramsay EA, Cunningham CH, Plewes DB, Temporal stability of adaptive 3D radial MRI using multidimensional golden means, Magn. Reson. Med 61 (2) (2009) 354–363, 10.1002/mrm.21837. [PubMed: 19165897]

[10]. Sekihara K, Steady-state magnetizations in rapid NMR imaging using small flip angles and short repetition intervals, IEEE Trans. Med. Imaging 6 (2) (1987) 157–164, 10.1109/TMI.1987.4307816. [PubMed: 18230442]

[11]. Goette MJ, Keupp J, Rahmer J, Lanza GM, Wickline SA, Caruthers SD, Balanced UTE-SSFP for ^{19}F MR imaging of complex spectra, Magn. Reson. Med 74 (2) (2015) 537–543, 10.1002/mrm.25437. [PubMed: 25163853]

[12]. Duyn JH, Steady state effects in fast gradient echo magnetic resonance imaging, Magn. Reson. Med 37 (4) (1997) 559–568, 10.1002/mrm.1910370414. [PubMed: 9094078]

[13]. Denolin V, Azizieh C, Metens T, New insights into the mechanisms of signal formation in RF-spoiled gradient echo sequences, Magn. Reson. Med 54 (4) (2005) 937–954, 10.1002/mrm.20652. [PubMed: 16155898]

[14]. Wei L, Hee KS, Improved signal spoiling in fast radial gradient-echo imaging: applied to accurate t1 mapping and flip angle correction, Magn. Reson. Med 62 (5) (2009) 1185–1194, 10.1002/mrm.22089. [PubMed: 19780174]

[15]. Zur Y, Wood ML, Neuringer LJ, Spoiling of transverse magnetization in steady-state sequences, Magn. Reson. Med 21 (2) (1991) 251–263, 10.1002/mrm.1910210210. [PubMed: 1745124]

[16]. Epstein FH, Mugler JP, Brookeman JR, Spoiling of transverse magnetization in gradient-echo (GRE) imaging during the approach to steady state, Magn. Reson. Med 35 (2) (1996) 237–245, 10.1002/mrm.1910350216. [PubMed: 8622589]

[17]. Weiger M, Brunner DO, Dietrich BE, Müller CF, Pruessmann KP, ZTE imaging in humans, Magn. Reson. Med 70 (2) (2013) 328–332, 10.1002/mrm.24816. [PubMed: 23776142]

[18]. Boucneau T, Fernandez B, Besson FL, et al., AZTEK: adaptive zero TE k-space trajectories, Magn. Reson. Med (2) (2020) 1–10, 10.1002/mrm.28483.

[19]. Roeloffs V, Voit D, Frahm J, Spoiling without additional gradients: radial FLASH MRI with randomized radiofrequency phases, Magn. Reson. Med 75 (5) (2016) 2094–2099, 10.1002/mrm.25809. [PubMed: 26094973]

[20]. Idiyatullin D, Corum C, Park JY, Garwood M, Fast and quiet MRI using a swept radiofrequency, J. Magn. Reson 181 (2) (2006) 342–349, 10.1016/j.jmr.2006.05.014. [PubMed: 16782371]

[21]. Willmering MM, Robison RK, Wang H, Pipe JG, Woods JC, Implementation of the FLORET UTE sequence for lung imaging, Magn. Reson. Med 82 (3) (2019), 10.1002/mrm.27800, mrm.27800.

[22]. Delacoste J, Chaptinel J, Beigelman-Aubry C, Piccini D, Sauty A, Stuber M, A double echo ultra short echo time (UTE) acquisition for respiratory motion-suppressed high resolution imaging of the lung, Magn. Reson. Med 79 (4) (2018) 2297–2305, 10.1002/mrm.26891. [PubMed: 28856720]

[23]. Jaynes ET, Matrix treatment of nuclear induction, Phys. Rev 98 (4) (1955) 1099–1105, 10.1103/PhysRev.98.1099.

[24]. Bloch F, Nuclear induction, Phys. Rev 70 (7–8) (1946) 460–474, 10.1103/PhysRev.70.460.

[25]. Weigel M, Extended phase graphs: dephasing, RF pulses, and echoes - Pure and simple, J. Magn. Reson. Imaging 41 (2) (2015) 266–295, 10.1002/jmri.24619. [PubMed: 24737382]

[26]. Tyler DJ, Robson MD, Henkelman RM, Young IR, Bydder GM, Magnetic resonance imaging with ultrashort TE (UTE) PULSE sequences: technical considerations, J. Magn. Reson. Imaging 25 (2) (2007) 279–289, 10.1002/jmri.20851. [PubMed: 17260388]

[27]. Cheng JY, Zhang T, Ruangwattanapaisarn N, et al., Free-breathing pediatric MRI with nonrigid motion correction and acceleration, J. Magn. Reson. Imaging 42 (2) (2015) 407–420, 10.1002/jmri.24785. [PubMed: 25329325]

[28]. Soustelle L, Lamy J, Rousseau F, Armspach J-P, Loureiro de Sousa P, A diffusion-based method for long-T_2 suppression in steady state sequences: validation and application for 3D-UTE imaging, Magn. Reson. Med 80 (2) (2018) 548–559, 10.1002/mrm.27057. [PubMed: 29266427]

[29]. Feng L, Delacoste J, Smith D, et al., Simultaneous evaluation of lung anatomy and ventilation using 4D respiratory-motion-resolved ultrashort echo time sparse MRI, J. Magn. Reson. Imaging 49 (2) (2019) 411–422, 10.1002/jmri.26245. [PubMed: 30252989]

[30]. Larson PEZ, Gurney PT, Nishimura DG, Anisotropic field-of-views in radial imaging, IEEE Trans. Med. Imaging 27 (1) (2008) 47–57, 10.1109/TMI.2007.902799. [PubMed: 18270061]

[31]. Krishnamoorthy G, Smink J, Tourais J, Breeuwer M, Kouwenhoven M, Variable anisotropic FOV for 3D radial imaging with spiral phyllotaxis (VASP), Magn. Reson. Med 85 (1) (2021) 68–77, 10.1002/MRM.28449. [PubMed: 32851711]

[32]. Zucker EJ, Cheng JY, Haldipur A, Carl M, Vasanawala SS, Free-breathing pediatric chest MRI: Performance of self-navigated golden-angle ordered conical ultrashort echo time acquisition, J. Magn. Reson. Imaging 47 (1) (2018) 200–209, 10.1002/jmri.25776. [PubMed: 28570032]

[33]. Johnson KM, Hybrid radial-cones trajectory for accelerated MRI, Magn. Reson. Med 77 (3) (2017) 1068–1081, 10.1002/mrm.26188. [PubMed: 27017991]

[34]. Robison RK, Anderson AG, Pipe JG, Three-dimensional ultrashort echo-time imaging using a FLORET trajectory, Magn. Reson. Med 78 (3) (2017) 1038–1049, 10.1002/mrm.26500. [PubMed: 27775843]
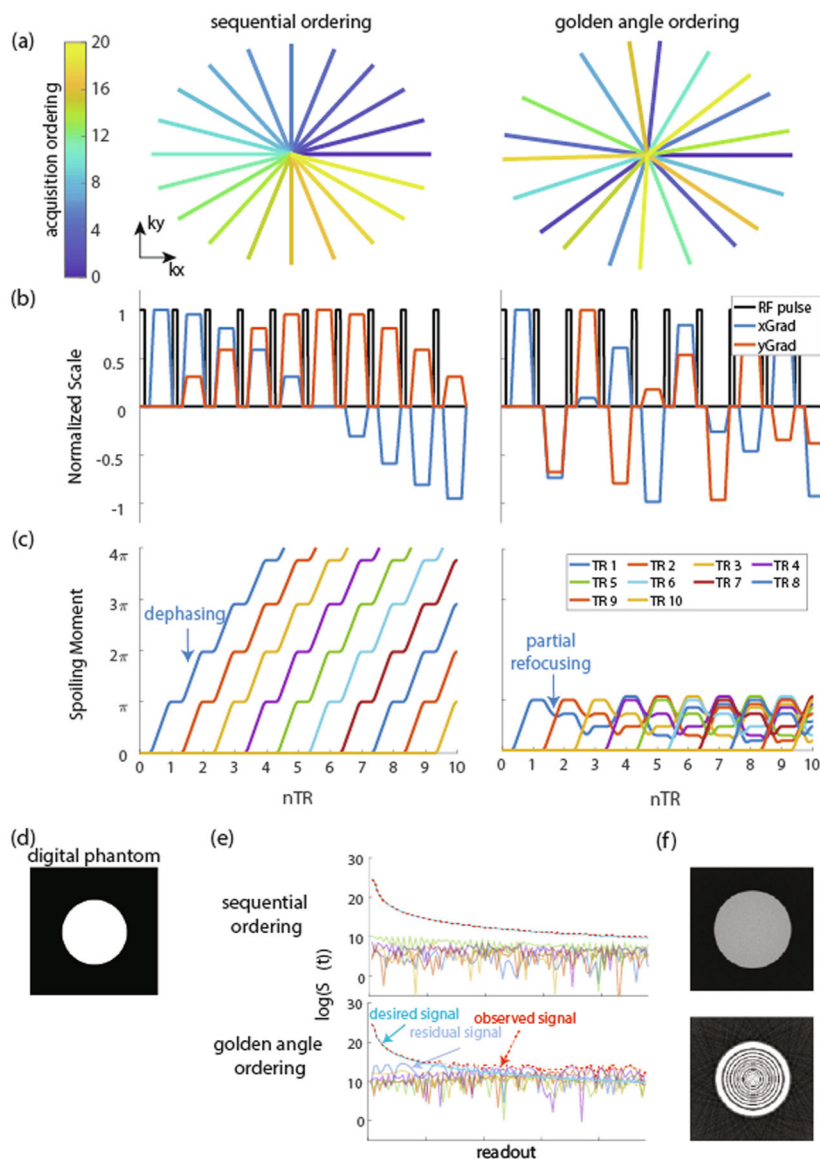
Fig. 1.
Effects of ordering design on spoiler gradient free 2D radial acquisitions. Sequential and golden angle ordering schemes with 20 spokes are plotted in (a). The corresponding sequence sketches are shown in (b). According to Equation (7, 8), spoiling moments induced by the encoding gradients of two different ordering schemes are plotted in (c). An digital phantom, (d), is used for 2D simulation comparison. Signal amplitudes from previous TRs in current readout are plotted in (e). Dashed red lines show the acquired signal, and signals from the current excitation as well as unwanted residual transverse signals from prior TRs. (f) shows the reconstructed images based on the simulated signals from (e).
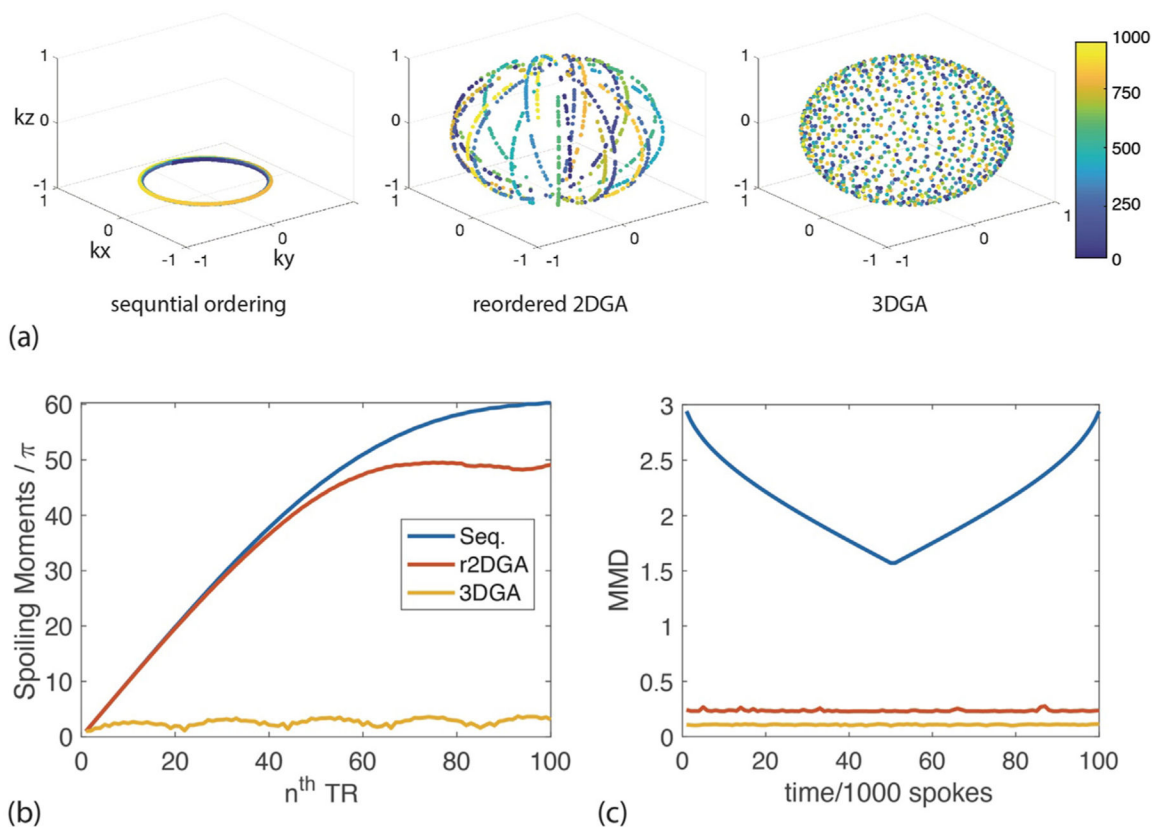
Fig. 2.
3D trajectory ordering schemes and spoiling effect analysis. 1000 continuous spokes from a trajectory with 100,000 spokes are plotted in (a), where the sequential acquisition only covers a small part of k-space (limiting robustness to motion), however, r2DGA and 3DGA schemes sample the k-space more uniformly. The average accumulated spoiling moments created by different schemes in the subsequent TRs are plotted in (b), demonstrating greater accumulation of spoiling effects in r2DGA and 3DGA. The maximum minimum distances (MMD) of different ordering schemes over time are plotted in (c), which quantifies the uniformity of the k-space sampling throughout the scan time.
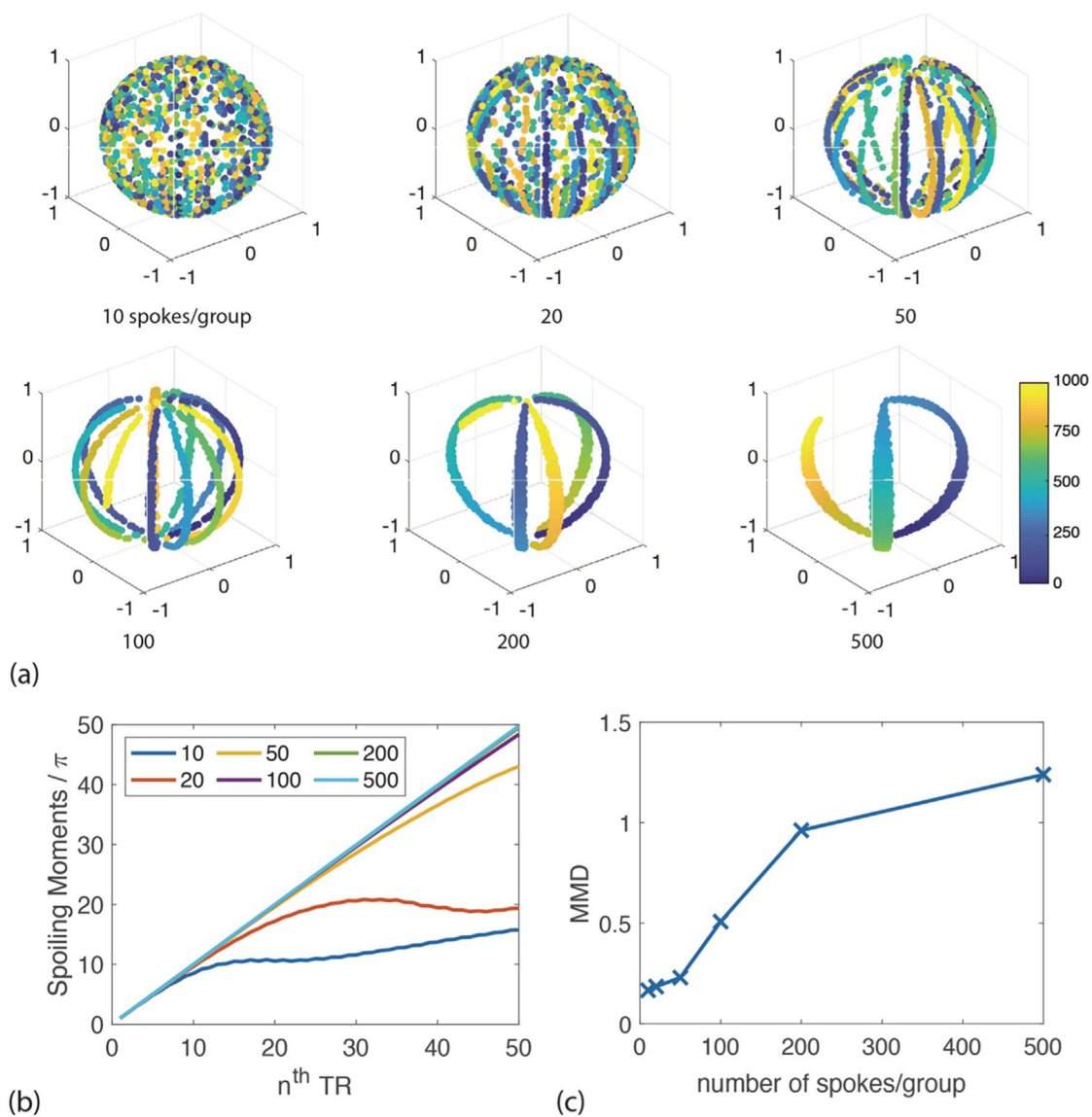
Fig. 3.
Illustration of the Number of spokes per group parameter in the r2DGA ordering design. 1000 spokes out of a 100,000 spoke trajectory with different number of spokes per group are plotted in (a), and the accumulated spoiling moments are plotted in (b). MMD of r2DGA with different number of spokes per group is shown in (c). With increasing spokes per group the accumulated spoiling moment increases but at the expense of reduced sampling uniformity.
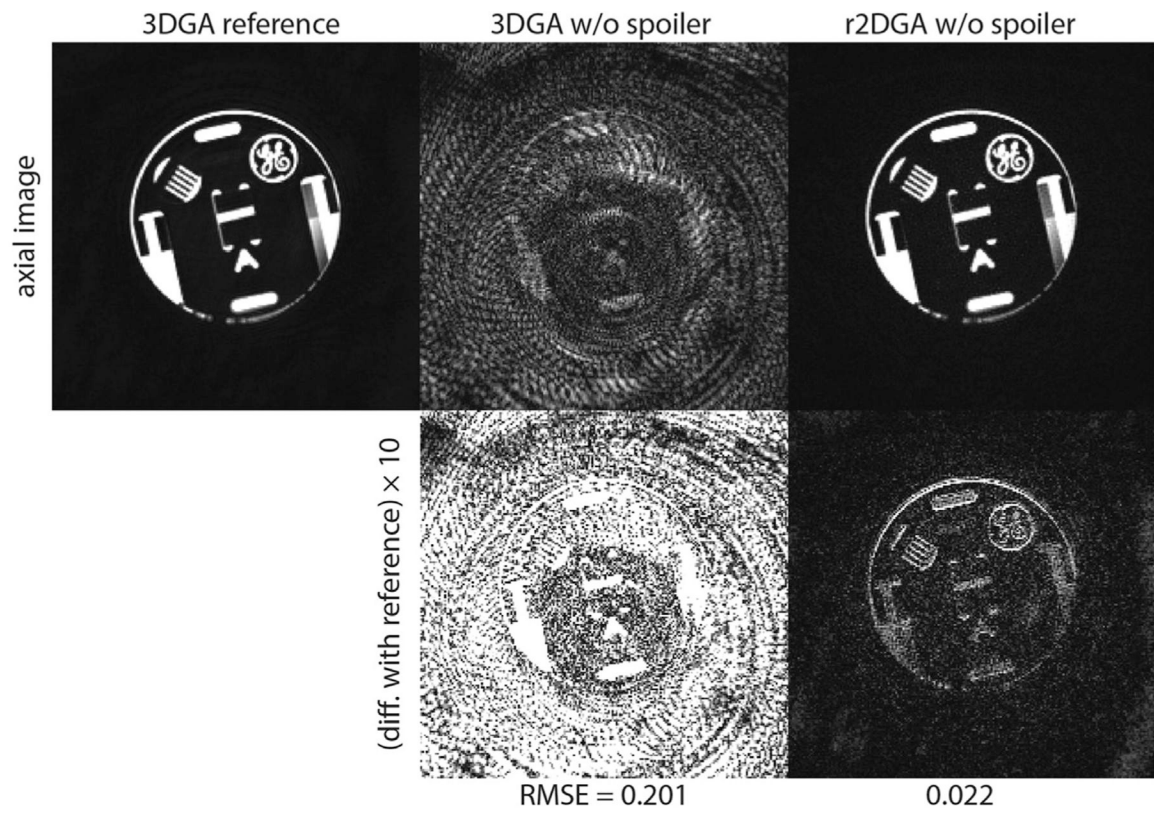
Fig. 4.
Phantom study with different ordering schemes without spoiler gradients. Images acquired with the reference sequence, the 3DGA without spoiler gradient, and the r2DGA without spoiler gradient are compared. Compared to reference scan, the image acquired with the r2DGA ordering scheme has relatively subtle noise-like artifacts, whereas the 3DGA without spoiler gradient shows strong artifacts compared to the other two, and the root mean square errors of difference with reference much higher.
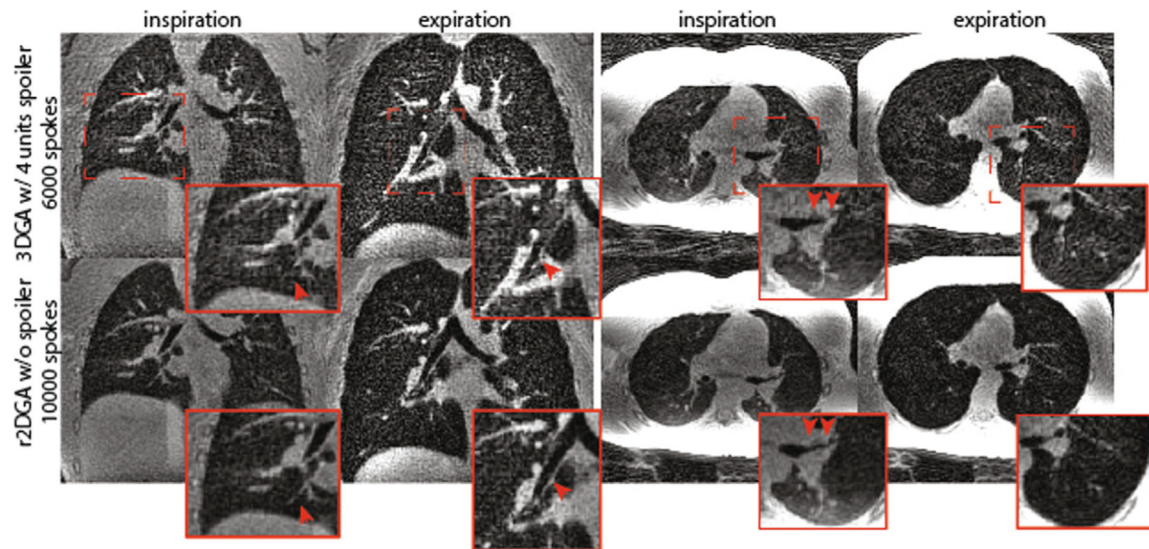
Fig. 5.
Breath-holding UTE lung imaging volunteer study. Two acquisition schemes, 3DGA with 4π spoiler gradient (6000 spokes, TR = 2.5 ms) and r2DGA without spoiler gradient (10,000 spokes, TR = 1.5 ms), were used to acquire breath-holding images in 15 s. Breath-holding at both inspiration and expiration were acquired. The r2DGA shows notably less streaking artifacts and clearer lung structures than 3DGA scheme (red arrows), likely because of reduced undersampling and reduced refocused magnetization.
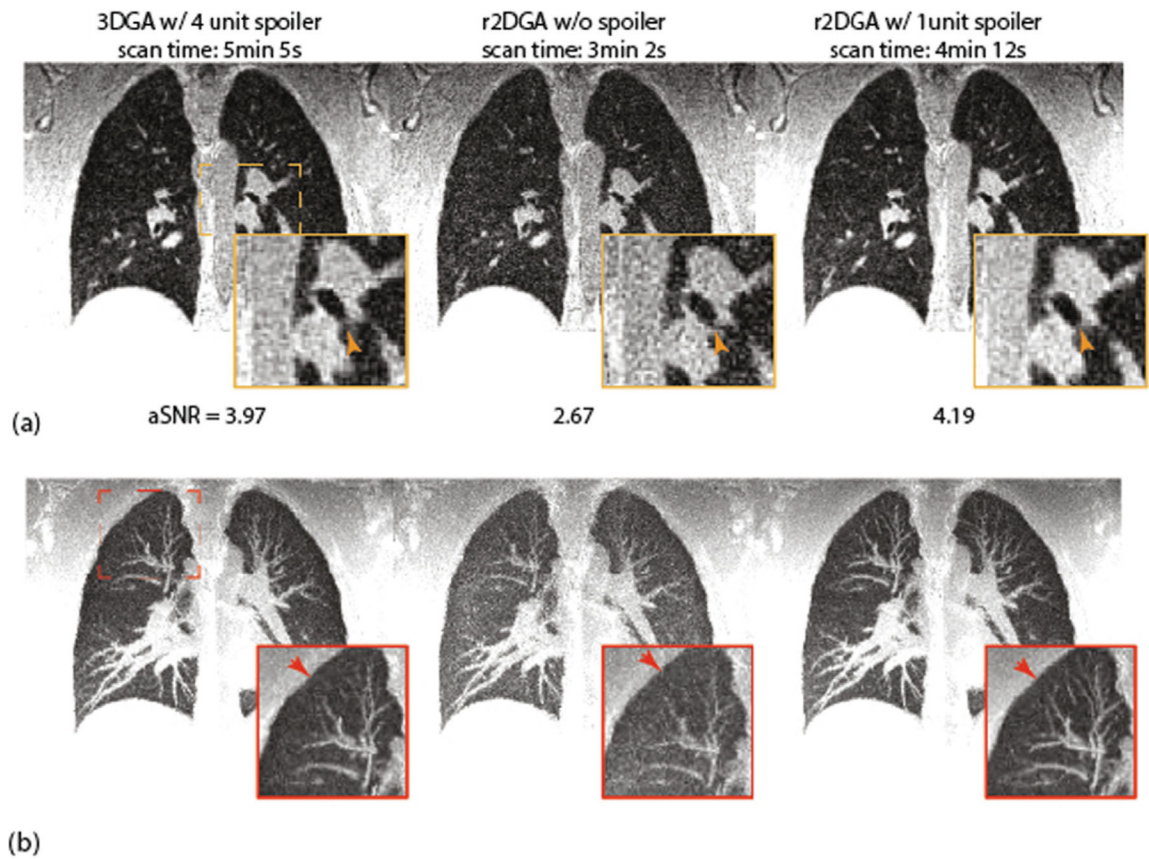
Fig. 6.
Free-breathing UTE lung imaging volunteer study. One coronal slice of 3D volume with different ordering schemes are shown in (a). The image acquired by the r2DGA without spoiler is slightly noisier than the 4 π spoiler scan, but the scan time was reduced by 40%. Maximum intensity projection (MIP) of 15 coronal slices from each volume are plotted in (b). The r2DGA scheme with a small 1 π spoiler gradient shows similar delineation of small vessels compared to the 4 π spoiler scan but with a 20% shorter scan time.